Avicenna Journal of Phytomedicine (AJP)

Original article

Zingiber officinale protects against acrylamide-induced spatial memory impairment, oxidative stress, and neurodegeneration in rats

Hamid Reza Moradi[1,*], Zabihollah Khaksar[1], Fatemeh Alipour[1], Saeid Fathollahi[1], Mahnaz Taherianfard[1], Mohsen Rashidi[1], Melika Khodayari[1]

[1]*Department of Basic Sciences, School of Veterinary Medicine, Shiraz University, Shiraz, Iran*

Article history:
Received: Sep 13, 2025
Received in revised form: Oct 23, 2025
Accepted: Feb 14, 2026
Epub ahead of print

**** Corresponding Author:***
Tel: +987136138652
Fax: +987132286940
hr.moradi@shirazu.ac.ir

Keywords:
Zingiber officinale
Acrylamide
Memory impairment
Oxidative stress
Neurodegeneration
Rats

Abstract

Objective: Acrylamide (ACA), an environmental and dietary contaminant, induces oxidative stress, neuroinflammation, and apoptosis, leading to cognitive impairment. This study investigated the neuroprotective potential of ginger (*Zingiber officinale)* hydroalcoholic extract (ZOE) against chronic ACA-induced neurotoxicity in rats.

Materials and methods: Thirty-two male Sprague-Dawley rats (n = 8 per group) were randomly assigned to four groups, each receiving a daily oral gavage for 52 days: healthy control (1 ml distilled water), ACA (10 mg/kg/day), ZOE (200 mg/kg/day), and ACA+ZOE (10 + 200 mg/kg/day). Spatial learning and memory were evaluated using the Morris water maze (MWM). Oxidative stress indices including total antioxidant capacity (TAC), total oxidant status (TOS), and oxidative stress index (OSI), as well as histomorphometric parameters and immunohistochemical (IHC) markers of apoptosis and gliosis (p53, Bcl-2, and GFAP) were assessed in the hippocampus and parietal cortex. Data were analyzed using one-way and two-way ANOVA, followed by Tukey's post hoc test.

Results: ACA exposure led to spatial memory acquisition impairment, accompanied by increased TOS and OSI, reduced TAC, decreased neuronal density and layer thickness, and upregulation of p53 and GFAP, and downregulation of Bcl-2 expression. ZOE co-administration markedly mitigated these effects by preserving neuronal architecture, restoring redox balance, and normalizing apoptosis- and gliosis-related protein expression.

Conclusion: Overall, our findings provide integrated behavioral, biochemical, histological, and molecular evidence supporting ZOE as a promising therapeutic candidate for environmentally induced neurotoxicity.

Please cite this paper as:
Moradi H.R, Khaksar Z, Alipour F, Fathollahi S, Taherianfard M, Rashidi M, Khodayari M. *Zingiber officinale* protects against acrylamide-induced spatial memory impairment, oxidative stress, and neurodegeneration in rats. Avicenna J Phytomed, 2026

Introduction

Exposure to environmental neurotoxicants has emerged as a critical public health concern because of their potential to cause progressive neural damage and persistent changes in brain functions. Among these compounds, acrylamide (ACA), a low–molecular weight, water-soluble molecule, has gained attention not only for its industrial applications but also for its unintended formation in carbohydrate-rich foods during high-temperature cooking methods such as frying, baking, and roasting (Zhao et al. 2022). Accumulating evidence underscores the public health relevance of ACA as a chemical agent with subtle but harmful effects. At the cellular level, ACA disrupts the redox balance in neural tissues, provoking excessive generation of reactive oxygen species (ROS), mitochondrial dysfunction, activation of intrinsic apoptotic pathways, and widespread structural and functional alterations in the neural architecture (Huchthausen et al. 2023; Moradi et al. 2025a). Acrylamide also damages the peripheral nervous system (PNS). Chronic exposure causes hindlimb weakness, gait abnormalities, and peripheral neuropathy in both rodents and humans (Zhao et al. 2022). However, central nervous system effects (such as hippocampal oxidative stress, apoptosis, and memory impairment) have also been reported, even in the absence of overt locomotor dysfunction (Izumi et al. 2022). Since these neuropathological alterations primarily affect the hippocampus, spatial learning and memory depend critically on the structural and functional integrity of its CA1, CA3, and dentate gyrus (DG) subregions, as well as on the posterior parietal cortex which integrates multisensory spatial cues (Save et al. 2005; Zhang and Jonas 2020). Disruptions within these regions compromise neural network coherence and degrade behavioral performance, as shown by hippocampal-dependent paradigms such as the Morris water maze (MWM) (Gomez-Pinilla and Hillman 2013). Despite substantial work outlining the deleterious effects of ACA, there remains a notable gap in studies identifying therapeutic interventions capable of addressing deficits at the behavioral, histological and molecular levels.

In recent decades, several naturally derived compounds with strong antioxidant, anti-inflammatory, and anti-apoptotic properties have garnered interest as potential neuroprotective agents (Shoaib et al. 2023; Negah et al. 2025). *Zingiber officinale* Roscoe (ginger), which is widely used in traditional therapies, exemplifies this therapeutic potential (Alshaer et al. 2025; Ojo et al. 2021). Its bioactive constituents including gingerols and shogaols, have demonstrated considerable efficacy in safeguarding neuroarchitecture and function in experimental models of brain injury and neurodegeneration (Arcusa et al. 2022; Ayinla and Asuku 2025).

Building on these findings, the present study investigated whether *Z. officinale* extract (ZOE) could attenuate ACA-induced impairment of spatial memory acquisition and prevent the associated structural brain damage in rats. Unlike previous reports that examined acute or isolated endpoints (Haidari et al. 2020; Mortazavi et al. 2025; Tandisehpanah et al. 2022), this study used an integrative approach that combined behavioral assays (MWM), quantification of oxidative stress parameters, including total antioxidant capacity (TAC), total oxidant status (TOS), and the oxidative stress index (OSI), histomorphometric evaluation, and immunohistochemical analysis of apoptosis- and gliosis-related markers (Bcl-2, p53, and GFAP). This study aimed to clarify the mechanisms underlying the neuroprotective effects of ZOE in the context of neurotoxic environmental exposure, within a chronic, low-dose ACA exposure model. This comprehensive design provides novel insights into the multi-level neuroprotection afforded by *Z.*

officinale against environmentally induced neurotoxicity.

Materials and Methods

Study design

This experimental *in vivo* study evaluated the potential neuroprotective effects of *Z. officinale* hydroalcoholic extract against acrylamide-induced neurotoxicity in adult male Sprague-Dawley rats. The study lasted for 52 consecutive days, following a one-week acclimatization period.

Chemicals and plant extract preparation

Acrylamide (purity ≥99.9%) was obtained from Merck (Germany). A hydroalcoholic extract of *Z. officinale* (ginger) was prepared using maceration extraction. The dried ginger rhizomes were ground into a fine powder and extracted with a hydroalcoholic solution (Gholampour et al. 2017). The extract was then concentrated and stored at 4°C until use.

Animals and grouping

Thirty-two healthy adult male Sprague-Dawley rats (weight, 200–230 g) were housed under standard laboratory conditions (21–24°C, 12-hr light/dark cycle, with *ad libitum* access to food and water). After a 7-day adaptation period, the animals were randomly assigned to four equal groups (n = 8 per group):

I. Control group: Received 1 ml of distilled water (vehicle for ACA and ZOE) daily via oral gavage.
II. ACA group: Received ACA at a dose of 10 mg/kg body weight per day via oral gavage, as described in previous studies (Abd Al Haleem et al. 2022).
III. ZOE group: Received ZOE at a dose of 200 mg/kg body weight per day via oral gavage (Shalaby and Hamowieh 2010).
IV. ACA+ZOE group: Received both ACA (10 mg/kg/day) and ZOE (200 mg/kg/day) via oral gavage.

The body weights of the rats were recorded daily to adjust the administered dose accordingly. On day 53 (24 hr after the final treatment), spatial learning and memory were assessed using the Morris water maze (MWM) task. After behavioral assessment, the animals were euthanized under deep anesthesia using ketamine (80 mg/kg) and xylazine (10 mg/kg, i.p.) and euthanized for the collection of brains. The brains were immediately dissected, rinsed, snap-frozen in liquid nitrogen, and stored at −80°C for biochemical analyses. Brain tissues were used to evaluate the oxidative and antioxidative status, including TAC, TOS, and OSI. For histological and immunohistochemical evaluations, brain tissues were fixed in 10% neutral-buffered formalin and embedded in paraffin blocks. An overview of the experimental workflow is presented in Figure 1.

Ethical approval

All procedures involving animals were conducted in accordance with the ethical standards of Shiraz University guidelines for the care and use of laboratory animals. The study protocol was approved by the Institutional Animal Care and Use Committee under the ethics code IR.USREC.1403.015.

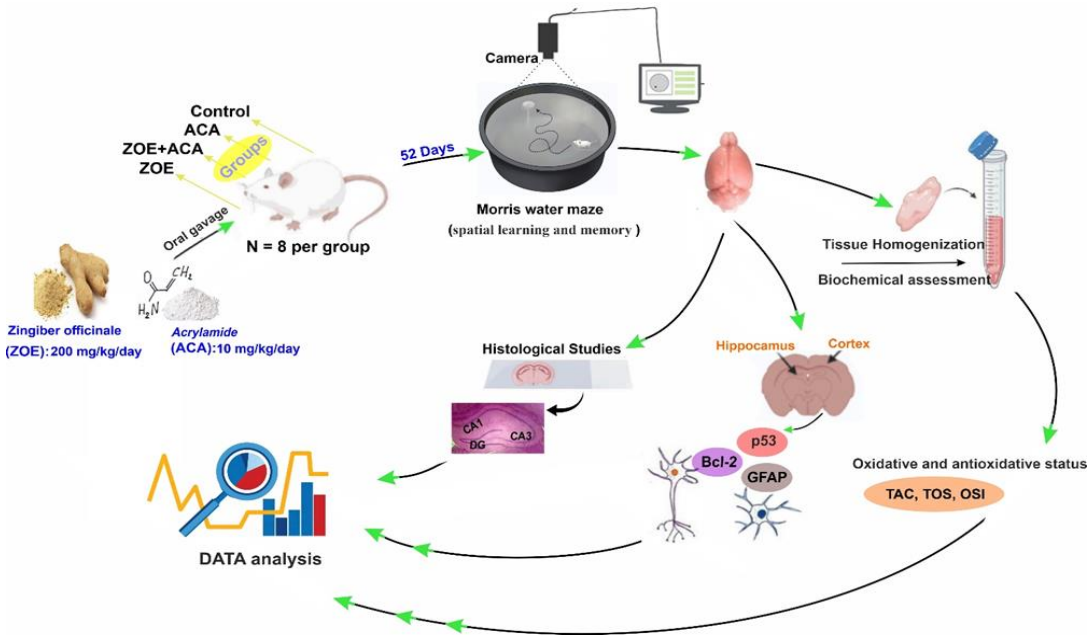

Figure 1. Schematic representation of the study design evaluating the neuroprotective effects of *Zingiber officinale* extract (ZOE) against acrylamide (ACA)-induced neurotoxicity in rats.

Behavioral assessment

To evaluate the effects of chronic ACA exposure and concurrent administration of ZOE on spatial learning, long-term memory, and motor function, the MWM task was conducted over a 7-day period. Behavioral experiments were conducted under controlled environmental conditions at the Physiology Laboratory of the Faculty of Veterinary Medicine, Shiraz University.

The maze consisted of a black circular pool (150 cm in diameter and 60 cm in height) filled with water to a depth of 40 cm, maintained at 26±1°C. A circular escape platform (10 cm² surface area) was positioned 4 cm below the water surface and remained in a fixed location during the hidden platform phase. Four distinct geometric visual cues were attached to the inner walls of the maze to facilitate spatial orientation. Animal trajectories were recorded using a ceiling-mounted digital camera and analyzed using NeuroVision software (Tajhiz Gostar Co., Iran), which was calibrated for this setup. All tests were conducted in a quiet room with consistent lighting (50 lux).

After 52 consecutive days of daily oral administration of ACA and/or ZOE, the animals underwent behavioral testing on days 53–59. During the 7-day testing period, no further administration of ACA, ZOE, or the vehicle (distilled water) was performed in any group, maintaining consistency with the chronic exposure design.

In this study, the MWM was conducted using a standard seven-day protocol: the first three days featured a visible platform phase for familiarization, followed by three days of hidden platform acquisition, and a final probe test on day seven after the platform was removed (Ahmadi et al. 2019).

Phase 1 – Visible Platform (Days 1–3): A visible platform trial was conducted over the first three days to assess baseline visual and motor abilities. The escape platform was marked with a white flag and remained in a fixed location throughout this phase. Each rat underwent four trials per day with randomized start positions (NE, NW, SE, and SW), always facing the pool wall. Each trial lasted up to 90 sec; if the rat did not locate the platform, it was gently guided to it and allowed to rest for 30 sec. The inter-trial interval was 30 sec. The key parameters recorded included escape

latency and swim velocity. Although the tracking software could also calculate distance traveled and path efficiency, in this study, we restricted our analysis to escape latency and swim velocity as the primary behavioral outcomes.

Phase 2 – Hidden Platform (Spatial Acquisition, Days 4–6): In this phase, the platform remained submerged (4 cm below the surface) and stayed in the same quadrant for all trials. Each rat completed four trials per day for three consecutive days with randomly assigned starting positions. A trial ended when the rat reached the platform or after 60 sec. Upon finding the platform, the rat was allowed to remain on it for 30 sec to encode the spatial cues from the environment. The animals were then gently removed, dried and returned to their home cages. After a 120-sec inter-trial interval, the next trial began in a different quadrant. The key parameters recorded included escape latency (time to reach the platform) and swim velocity (as an index of motor function).

Phase 3 – Probe Trial (Day 7): To assess long-term spatial memory, a 60-sec probe trial was conducted 24 hr after the final acquisition trial. The platform was removed, and the rats were released into the quadrant opposite the original platform location. Each rat swam freely for 60 sec before being removed, dried and returned to its home cage. After a 120-sec interval, the next animal was tested. The parameters analyzed included escape latency (time to reach the software-defined virtual platform zone) and swim velocity (to control for motor impairment).

The virtual platform location was defined in the tracking software based on the exact coordinates obtained from previous trials. When a rat crossed this virtual location, the software automatically recorded the event and terminated the trial. This design enabled an unbiased assessment of spatial memory without any reinforcement.

Motor function control: Swim velocity was continuously monitored across all testing phases to exclude motor deficits as potential confounding factors in this study. Group comparisons on the final day of acquisition confirmed that the differences in escape latency and memory performance were driven by spatial learning effects rather than locomotor impairments. All behavioral assessments were conducted by an experimenter blinded to the treatment groups.

Brain tissue homogenization

After behavioral testing, the brain tissue specimens were rapidly removed and dissected on ice. The forebrain, excluding the cerebellum and olfactory bulbs, was quickly frozen in liquid nitrogen and stored at −80°C for biochemical assays. Brains were homogenized in 250 µl of radioimmunoprecipitation assay (RIPA) lysis buffer [150 mM NaCl, 0.1% Sodium dodecyl sulfate (SDS), 25 mM Tris-HCl pH 7.4, 1 mM NaF, 1 mM phenylmethylsulfonyl fluoride (PMSF), 50 mM sodium fluoride] with a protease inhibitor cocktail (Sigma, USA) using a Heidolph homogenizer (Germany). Homogenates were centrifuged at 10,000 × g for 15 min at 3°C. The clear supernatants were collected, aliquoted, and stored at −80°C until analysis. Protein concentration was determined using the Bradford assay (Hosseinkhani et al., 2024).

Assessment of oxidative and antioxidative status

Total oxidant status (TOS) was measured using a semi-automated colorimetric method in a microplate format, with hydrogen peroxide (H_2O_2) as the calibration standard. The assay was performed according to a previously validated protocol (Bostanifard et al. 2026). The final TOS concentrations were normalized to the tissue protein content and expressed as µmol H_2O_2 equivalents per milligram of protein.

The TAC was determined using the ferric reducing antioxidant power (FRAP) assay, according to established protocols

reported in previous studies (Hosseinkhani et al. 2024). The working FRAP reagent was freshly prepared by mixing acetate buffer, TPTZ solution (2,4,6-tripyridyl-s-triazine) in hydrochloric acid (HCl), and ferric chloride ($FeCl_3$). Then, 10 µl of each homogenized brain sample was added to 290 µl of the FRAP reagent, incubated at room temperature for 10 min, and absorbance was measured at 593 nm. Vitamin C was used as a standard reference, and the results are reported as µmol of vitamin C equivalents per mg of protein.

The OSI was calculated as the ratio of TOS to TAC, multiplied by 100, and served as an integrated marker of redox imbalance severity (Hosseinkhani et al. 2024).

Protein quantification by Bradford assay

Protein content was measured using the Bradford method (Bradford 1976), which is based on the binding of Coomassie Brilliant Blue G-250 dye to proteins in acidic conditions. In a 96-well plate, 20 µl of tissue homogenate or distilled water (blank) was mixed with 40 µl of Bradford reagent and 140 µl of distilled water. After 10 min of incubation at room temperature, the absorbance was measured at 495 nm using a microplate reader (BioTek, USA). A standard curve was created using BSA (2–100 µg/ml), and the protein concentrations were calculated using linear regression. Final values are expressed as µg/ml and used to normalize the TAC and TOS measurements.

Histological and histomorphometric analysis

Following brain fixation, standard histological processing was performed using an automated tissue processor which included sequential dehydration, clearing, and paraffin embedding. Coronal sections of the hippocampus and parietal cortex were prepared using a rotary microtome at thicknesses of 6 µm for morphometric assessments and 3 µm for immunohistochemical (IHC) analyses. To evaluate the general tissue morphology and cytoarchitecture, coronal sections were stained with hematoxylin and eosin (H&E). Quantitative histomorphometric assessments were performed in predefined hippocampal subregions, focusing on (i) the thickness of the molecular and granular layers in the dentate gyrus (DG), (ii) the thickness of the stratum pyramidale in the CA1 and CA3 subfields, and (iii) neuronal density within the pyramidal layers of CA1 and CA3 and within the granular layer of the DG. All measurements were conducted using standardized histomorphometric methods to ensure unbiased estimates of neuronal density and layer thickness (Moradi et al. 2025a; Zhao and van Praag 2020). Microscopic evaluations were conducted using an Olympus light microscope (Olympus, Japan) equipped with a calibrated EC5R 10.0 MP eyepiece camera (China) and Keview software (China). For each animal, a minimum of 10 randomly selected, non-overlapping fields from at least two anatomically matched sections were analyzed for each sub-region. All data are presented as mean ± standard deviation (SD).

To assess neuronal density, stained brain sections were analyzed at ×400 magnification. Cell counts were performed using standardized square counting frames (100 × 100 µm; area = 0.01 mm^2). Although individual counts were obtained within these 0.01 mm^2 frames, the final results were normalized and expressed as the number of neurons per 1 mm^2 to ensure standardization and facilitate comparative analysis. Only neurons exhibiting clearly defined nuclear borders and characteristic morphological features were included in this study. In each hippocampal subregion, at least 10 fields were assessed for each animal. Neuronal density was calculated by dividing the total number of neurons counted by the total area examined and expressed as cells/mm^2. Counting was performed by an observer blinded to group allocation to eliminate observer bias.

The layer thickness was determined at ×100 and ×400 magnifications using the

same microscope. For each animal, at least 20 random, non-overlapping measurement points were recorded across each subregion (CA1, CA3, and DG) to ensure an anatomical representation. In the CA1 and CA3 regions, the thickness of the stratum pyramidale was measured from the upper to lower boundary. In the DG, the granular cell layer was measured from the inner to the outer border of the densely packed granular cell band. The molecular layer thickness was measured from the outer edge of the granular cell layer to the hippocampal fissure. All thickness measurements are expressed in micrometers (μm). To ensure objectivity, all analyses were conducted by an experimenter blinded to the experimental groups.

Immunohistochemistry staining

Immunohistochemical (IHC) staining was performed on 3 μm-thick brain sections to assess the expression of the following markers: Bcl-2 (anti-apoptotic), p53 (pro-apoptotic), and GFAP (glial fibrillary acidic protein, an astrocyte marker). All primary antibodies and detection kits were obtained from Elabscience (USA) and used according to the manufacturer's instructions. The three markers (p53, Bcl-2, and GFAP) were quantified by measuring the percentage of the 3,3′-diaminobenzidine (DAB)-stained area within each region of interest. Digital images were captured at 40× magnification, and the area of positive staining was analyzed using the ImageJ software (version 1.47; NIH, USA). The positivity index was expressed as the percentage of the total field area occupied by p53-, Bcl-2-, and GFAP-positive staining in the tissue (Moradi et al. 2026). For each hippocampal subregion and the parietal cortex, at least 10 non-overlapping fields were analyzed for each animal brain. Data are presented as mean ± standard deviation (SD).

Statistical analysis

Statistical analyses were performed using SPSS (version 26; IBM, USA). All data are presented as mean ± standard deviation (SD). Escape latency and swimming velocity in the MWM were analyzed using two-way repeated-measures ANOVA, with treatment group as the between-subject factor and training day as the within-subject factor. Separate analyses were performed for the visible (days 1–3) and hidden (days 4–6) platform phases. Significant main effects or group × day interactions were followed by Tukey's post hoc tests. Probe-trial latency, oxidative stress indices, histomorphometric variables, and immunohistochemical markers were compared across groups using one-way analysis of variance (ANOVA), followed by Tukey's post-hoc test. A p-value ≤ 0.05 was considered statistically significant.

Results

Effect of ZOE on spatial learning, memory, and motor function following ACA-induced neurotoxicity

Spatial learning: Escape latency data from the 7-day MWM test revealed significant intergroup differences in spatial learning. During the visible-platform phase (days 1–3), ACA-treated rats had longer escape latencies than controls starting on day 1 (73.84 ± 4.34 vs. 39.60 ± 6.55 sec; $p<0.001$). Latency declined with training in all groups, but ACA animals remained slower than controls through day 6 (45.16 ± 7.23 vs. 14.10 ± 3.64 sec; $p<0.001$), indicating impaired but not absent learning. Rats receiving ACA + ZOE showed progressive improvement (day 2: 49.11 ± 4.33 and day 5: 16.01 ± 1.63 sec; $p < 0.001$ vs. ACA) and, by day 6, had shorter latencies than controls (10.44 ± 4.78 vs. 14.10 ± 3.64 sec; $p>0.05$). The ZOE-only group performed comparably to the controls across all phases, indicating that ZOE administration alone did not adversely

affect spatial memory acquisition or retention (Figure 2A).

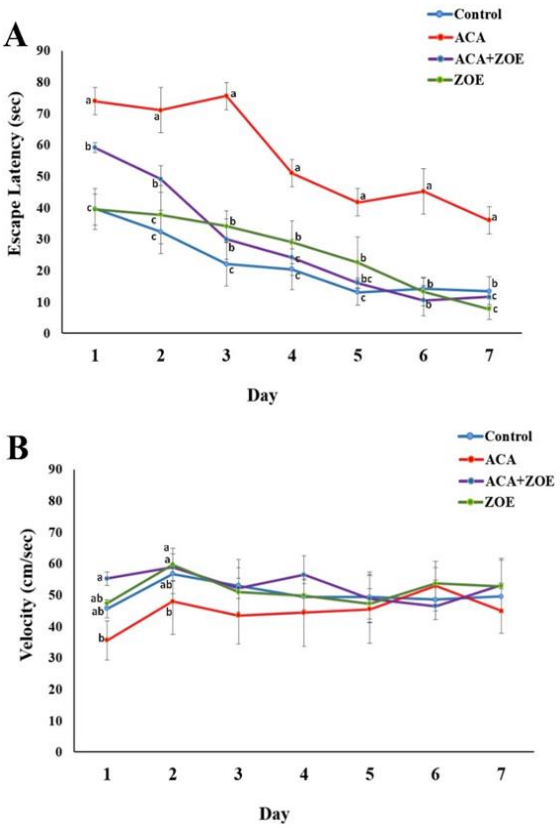

Figure 2. Effects of acrylamide (ACA) and *Zingiber officinale* extract (ZOE) on spatial learning performance in the Morris water maze test. (A) Escape latency (s) and (B) swimming velocity (cm/s) over seven consecutive training days (visible platform: days 1–3; hidden platform: days 4–6; probe trial:day 7). Data are presented as the mean ± standard deviation (n=8/group). Different lowercase letters (a, b, and c) indicate statistically significant differences among groups (two-way repeated-measures ANOVA followed by Tukey's post-hoc test, $p<0.05$). The ACA group exhibited significantly prolonged escape latencies from day 2 onward, which indicated impaired spatial learning. However, co-administration of ZOE (ACA+ZOE) progressively reduced the latencies to control levels by day 5 post-treatment. On the first day, ACA-treated rats showed a slightly reduced swimming velocity, suggesting a minor motor impairment. From the third day onward, however, no significant differences were observed among the groups, indicating that the primary deficits induced by ACA were central, particularly affecting spatial learning and memory.

Swimming velocity (motor function): Velocity measurements were included to control for potential non-cognitive confounding factors related to locomotor performance.

On day 1, no significant difference was observed between controls (45.64 ± 2.87 cm/sec) and ACA rats (35.54 ± 6.20 cm/sec; $p>0.05$), but all other groups swam faster than ACA animals. The ACA+ZOE group (55.16 ± 2.17 cm/sec) showed a significant increase in velocity on day 1 compared with ACA ($p<0.05$). On day 2, both ACA+ZOE (58.76 ± 4.19 cm/sec) and ZOE-only (59.59 ± 5.19 cm/sec) rats maintained higher velocities than ACA (47.86 ± 10.42 cm/sec; $p<0.05$). By the third visible session, swimming speeds no longer differed among groups. On Day 6, all groups exhibited similar velocities, indicating that the differences in escape latency were not due to motor impairment (Figure 2B).

Probe trial (memory retention): Twenty-four hours after training (Day 7), memory retention was assessed using a probe trial. ACA-treated rats showed significantly longer latency (32.5 ± 3.4 sec) to reach the virtual platform than controls (18.2 ± 2.1 sec, $p<0.01$), indicating memory deficits. The ACA+ZOE group showed partial rescue of spatial memory acquisition (28.7 ± 2.9 sec, $p < 0.05$ vs. ACA group), whereas the ZOE-only group performed equivalently to controls, supporting both the safety and potential memory-enhancing properties of ZOE (Figure 2).

Effect of ZOE on oxidative and antioxidative status following ACA-induced neurotoxicity

The results of the present study demonstrated significant alterations in oxidative stress parameters across the treatment groups. Rats exposed to ACA showed a substantial reduction in TAC compared to the control group (2.54 ± 0.16 vs. 4.13 ± 0.48 µmol vitamin C equivalent/mg protein, $p<0.01$), indicating a pronounced suppression of the endogenous antioxidant defense system. Interestingly, the ZOE group (4.46 ± 0.19 µmol vitamin C Eq/mg protein) exhibited a

numerically higher TAC than the control group, although this difference was not statistically significant, suggesting a potential baseline enhancement of the antioxidant status (Figure 3A).

Conversely, TOS was significantly elevated in the ACA group (0.14 ± 0.02 vs. 0.05 ± 0.005 µmol H_2O_2 equivalent/mg protein in the control group, $p<0.001$), confirming ACA-induced oxidative stress. The ZOE-only group (0.057 ± 0.007 µmol H_2O_2 Eq/mg protein) maintained TOS levels comparable to the control group, indicating that ZOE administration alone did not induce oxidative stress (Figure 3B).

The OSI, calculated as the TOS/TAC ratio × 100, was markedly increased in the ACA group (5.6 ± 0.92 vs. 1.53 ± 0.44 in the control group, $p<0.001$), highlighting a severe redox imbalance. Notably, the ZOE-alone group exhibited the lowest OSI value (1.28 ± 0.14), even below the control levels, although this difference was not statistically significant (Figure 3C).

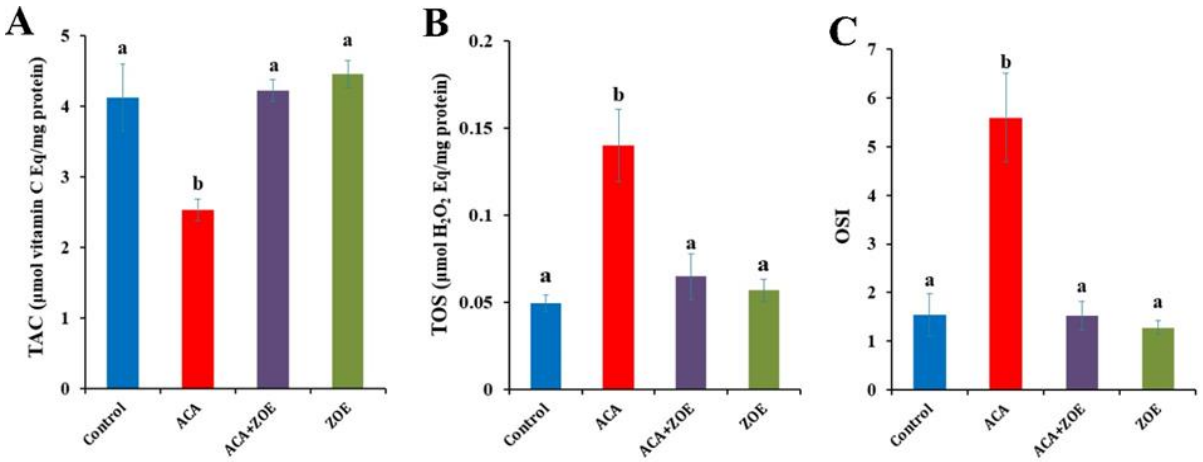

Figure 3. Effects of acrylamide (ACA) and *Zingiber officinale* extract (ZOE) on oxidative and antioxidative status in rat brain tissue. (A) Total antioxidant capacity (TAC), (B) total oxidant status (TOS), and (C) oxidative stress index (OSI) in the experimental groups. Data are presented as the mean ± standard deviation. Different lowercase letters (a, b, and c) indicate statistically significant differences among groups (one-way ANOVA followed by Tukey's post-hoc test, $p<0.05$).

Effect of ZOE on histometrical analysis following ACA-induced neurotoxicity

The pyramidal layer thickness in both CA1 and CA3 was significantly reduced following ACA exposure (CA3: 55.08 ± 6.11 µm and CA1: 52.56 ± 5.21 µm) compared to control values (CA3: 72.13 ± 10.17 µm and CA1: 63.78 ± 6.68 µm). Co-administration of ZOE significantly improved layer thickness (ACA+ZOE: CA3:75.33 ± 10.28 µm and CA1:60.42 ± 4.02 µm), indicating partial structural recovery. The ZOE-only group exhibited the highest thickness values among all the groups (Figure 4).

In the ACA group, the thickness of both the molecular and granular layers of the DG was significantly reduced compared to that in the control group ($p<0.001$). Specifically, the molecular layer thickness decreased from 220.95 ± 8.54 µm (control) to 175.85 ± 10.73 µm (ACA). Similarly, the granular layer showed a marked reduction from 74.63 ± 8.23 µm in the control group to 52.44 ± 7.26 µm in the ACA group. Co-treatment with ZOE and ACA significantly restored the layer thickness, with a statistically significant improvement compared to ACA alone and no significant difference from that of the control group. Notably, the ZOE-only group exhibited higher thickness values than the control group, although this difference was not statistically significant (Figure 4).

ACA treatment resulted in a significant decrease in neuronal density in all examined subregions: CA1 (1433 ± 87 cells/mm²), CA3 (1312 ± 55 cells/mm²), and DG (1774 ± 115 cells/mm²) compared to the control values (CA1:1622 ± 87;

CA3:1437 ± 93 and DG: 2204 ± 77; p<0.001). Co-treatment with ZOE restored neuronal counts in all regions to levels close to those of the control group and, in some cases, significantly higher than those with ACA alone. The ZOE-only group exhibited the highest neuronal density overall, although the differences from the control group were not always statistically significant (Figure 4).

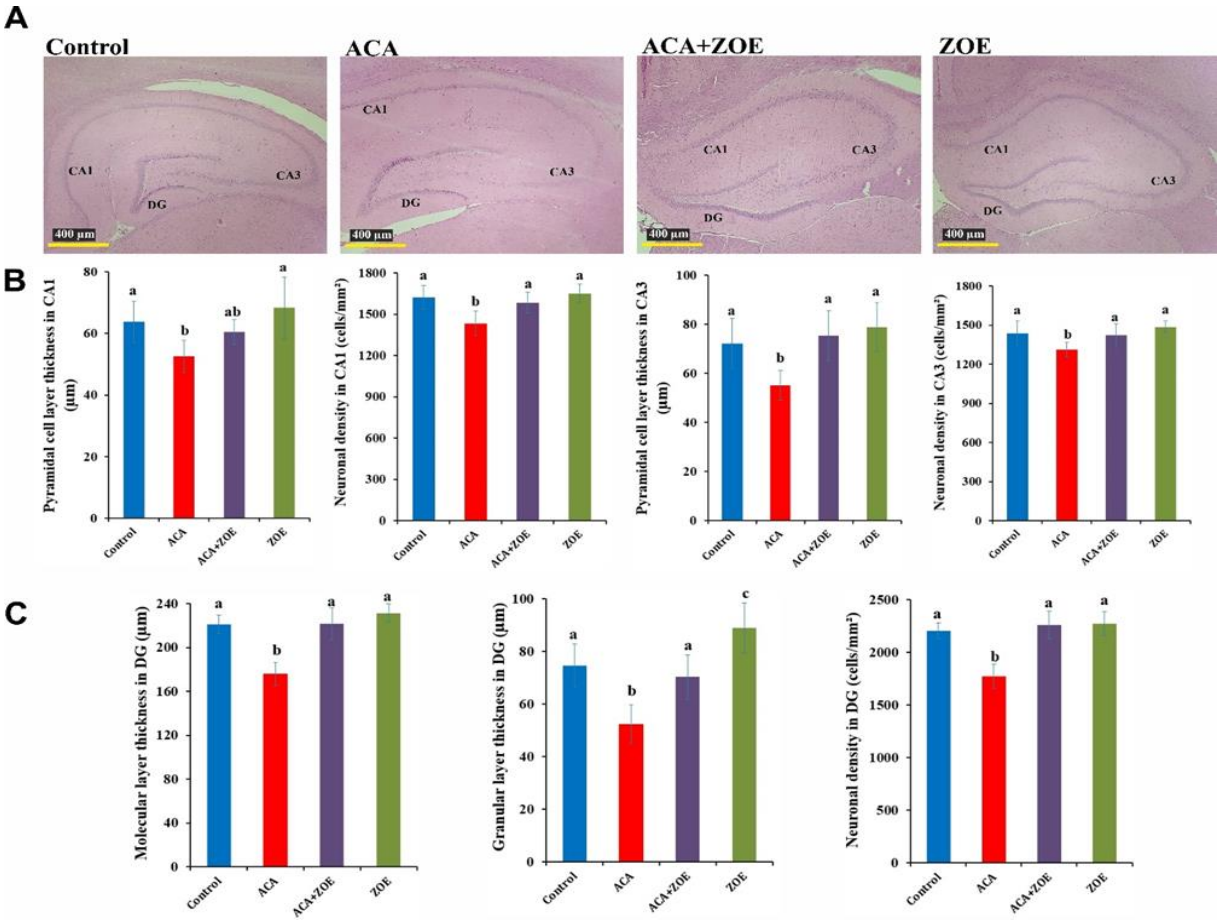

Figure 4. Histomorphometric assessment of hippocampal subregions following chronic acrylamide (ACA) exposure and/or *Zingiber officinale* extract (ZOE) treatment. (A) Representative hematoxylin and eosin (H&E)-stained sections showing the CA1, CA3, and dentate gyrus (DG) regions in the control, ACA, ACA+ZOE, and ZOE groups (magnification ×40; scale bar = 400 µm). (B) Quantitative measurements of pyramidal cell layer thickness and neuronal density in the CA1 and CA3 regions of the hippocampus. (C) Quantitative measurements of molecular layer thickness, granular layer thickness, and neuronal density in the DG. ACA treatment resulted in significant reductions in layer thickness and neuronal density in the CA1, CA3, and DG compared with the controls. Co-administration of ZOE and ACA markedly attenuated these alterations, restoring the values to those of the control group. ZOE alone did not significantly alter any of the measured parameters compared to the controls, indicating the absence of adverse morphological effects. Data are presented as the mean ± standard deviation. Different lowercase letters (a, b, and c) indicate statistically significant differences among groups (one-way ANOVA followed by Tukey's post-hoc test, p<0.05).

Effect of ZOE on p53, Bcl-2, and GFAP expression after ACA-induced CA1 neurotoxicity

In the CA1 region, the percentage of the p53-positive area significantly increased in the ACA group (12.50 ± 3.72%) compared to that in the control group (4.16 ± 0.79%) (p<0.001), indicating a robust induction of apoptotic marker expression after ACA exposure. Co-treatment with ZOE in the ACA+ZOE group reduced p53 levels to 4.47 ± 0.93%, approaching those of the control group (p>0.05). The ZOE-only group (3.57 ± 1.11%) showed slightly

lower values than the controls, but the difference was not significant. Bcl-2 expression in the CA1 region, Bcl-2 levels were significantly decreased in the ACA group (6.91 ± 1.70%) compared to the control group (10.43 ± 3.02%) ($p<0.01$), reflecting the suppression of this anti-apoptotic protein. Co-treatment with ZOE in the ACA+ZOE group partially restored Bcl-2 expression to 7.85 ± 1.15%, while the ZOE-only group (11.16 ± 1.57%) showed slightly higher levels than the controls, with no significant difference. GFAP expression in the CA1 region, GFAP expression significantly increased in the ACA group (53.53 ± 5.01%) compared to that in the control group (30.04 ± 0.49%) ($p<0.001$), indicating astrogliosis. Co-treatment with ZOE reduced GFAP to 27.36 ± 2.20% ($p<0.001$ vs. ACA), whereas the ZOE-only group exhibited lower levels than those in the control group (25.54 ± 1.85%) (Figure 5).

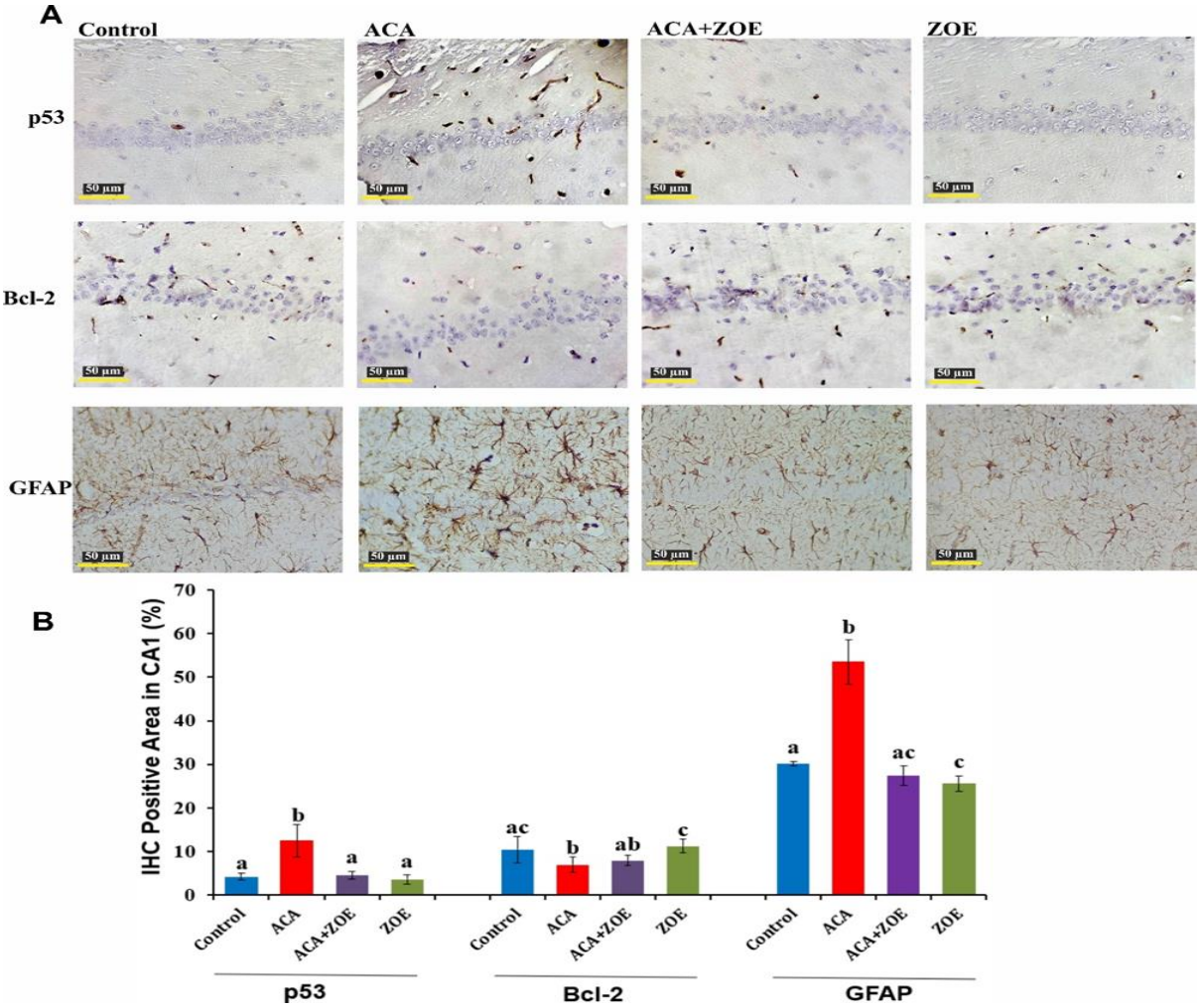

Figure 5. Immunohistochemical (IHC) analysis of p53, Bcl-2, and GFAP expression in the CA1 region following chronic acrylamide (ACA) exposure and/or *Zingiber officinale* extract (ZOE) administration. (A) Representative photomicrographs showing p53, Bcl-2, and GFAP immunoreactivity in the CA1 region across the experimental groups: Control, ACA, ACA+ZOE, and ZOE. ACA-treated rats showed marked increases in p53 and GFAP immunopositivity compared to the controls, whereas Bcl-2 expression was reduced. Co-treatment with ZOE attenuated ACA-induced p53 and GFAP overexpression and partially restored Bcl-2 levels. ZOE alone did not markedly alter the expression profile compared to that of the control group (magnification ×400; scale bar = 50 µm). (B) Quantification of the IHC-positive area (%) for each marker in CA1. Data are presented as mean ± standard deviation. Data are presented as the mean ± standard deviation. Different lowercase letters (a, b, and c) indicate statistically significant differences among groups (one-way ANOVA followed by Tukey's post-hoc test, $p<0.05$).

Effect of ZOE on p53, Bcl-2, and GFAP expression after ACA-induced CA3 neurotoxicity

In the CA3 region, ACA administration resulted in a marked elevation in p53 expression (14.02 ± 3.58%) relative to that in the control group (2.54 ± 0.89%) ($p < 0.001$). The ACA+ZOE group exhibited a significant reduction (6.02 ± 0.82%) compared to ACA alone ($p < 0.001$), whereas the ZOE-only group exhibited the lowest expression (1.97 ± 0.86%). In the CA3 region, ACA reduced Bcl-2 expression (7.39 ± 1.51%) compared to the control (12.19 ± 2.49%) ($p < 0.001$). The ACA+ZOE group (9.95 ± 1.16%) demonstrated a significant increase relative to the ACA alone group ($p<0.05$) but remained below the control levels. The ZOE-only group (12.15 ± 1.98%) showed comparable results to the control group. In the CA3 region, GFAP was elevated in the ACA group (58.13 ± 5.01%) compared to that in the control group (45.49 ± 3.04%) ($p<0.001$). The ACA+ZOE group showed a significant reduction (49.23 ± 4.86%) compared to the ACA group ($p < 0.001$), and the ZOE-only group had slightly lower levels than the controls (43.10 ± 4.33%) (Figure 6).

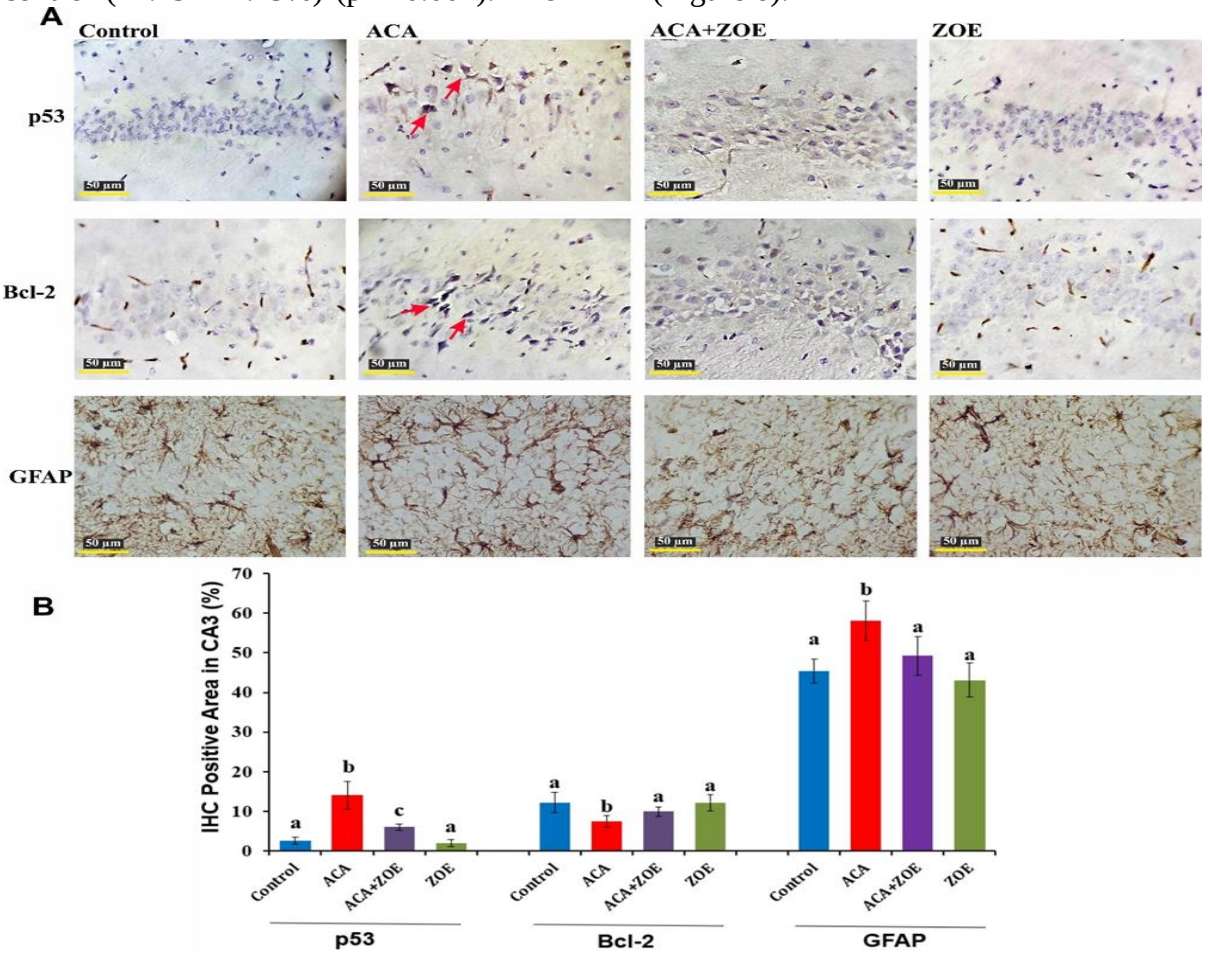

Figure 6. Immunohistochemical (IHC) analysis of p53, Bcl-2, and GFAP expression in the CA3 region following chronic acrylamide (ACA) exposure and/or *Zingiber officinale* extract (ZOE) administration. (A) Representative photomicrographs of p53, Bcl-2, and GFAP in the CA3 region of the control, ACA, ACA+ZOE, and ZOE groups. ACA increased p53 and GFAP levels and decreased Bcl-2 levels compared to those in the control. ZOE co-treatment reduced ACA-induced p53 and GFAP overexpression and partially restored Bcl-2 expression. ZOE alone showed no notable changes compared with the control. Red arrows indicate shrunken necrotic neurons with pyknotic nuclei (magnification ×400; scale bar = 50 µm). (B) Quantification of the IHC-positive area (%) for each marker in CA3. Data are presented as the mean ± standard deviation. Different lowercase letters (a, b, c) indicate statistically significant differences among groups (one-way ANOVA followed by Tukey's post-hoc test, $p<0.05$).

Effect of ZOE on p53, Bcl-2, and GFAP expression after ACA-induced DG neurotoxicity

In the dentate gyrus (DG), p53 expression was significantly higher in the ACA group (8.51 ± 2.28%) than in the control group (3.11 ± 0.74%) ($p<0.001$). Treatment with ZOE decreased p53 expression to 4.34 ± 0.64% in the ACA+ZOE group, while the ZOE-only group (2.93 ± 0.77%) remained at the control level. In the DG, Bcl-2 expression was significantly lower in the ACA group (10.04 ± 1.52%) than in the control group (13.64 ± 1.91%) ($p<0.001$). ZOE co-treatment elevated Bcl-2 to 11.56 ± 1.97 %, and the ZOE-only group (14.11 ± 1.38%) slightly exceeded the control values. In the DG, GFAP levels were significantly increased in the ACA group (63.56 ± 2.91%) compared to the control group (46.86 ± 2.57%) ($p<0.001$). ZOE co-treatment reduced GFAP expression to 54.93 ± 2.26% ($p<0.001$ vs. ACA), although the levels remained elevated compared to that in the control group ($p<0.01$). The ZOE-only group exhibited decreased GFAP expression (41.60 ± 3.31%) compared to the control group ($p<0.01$) (Figure 7).

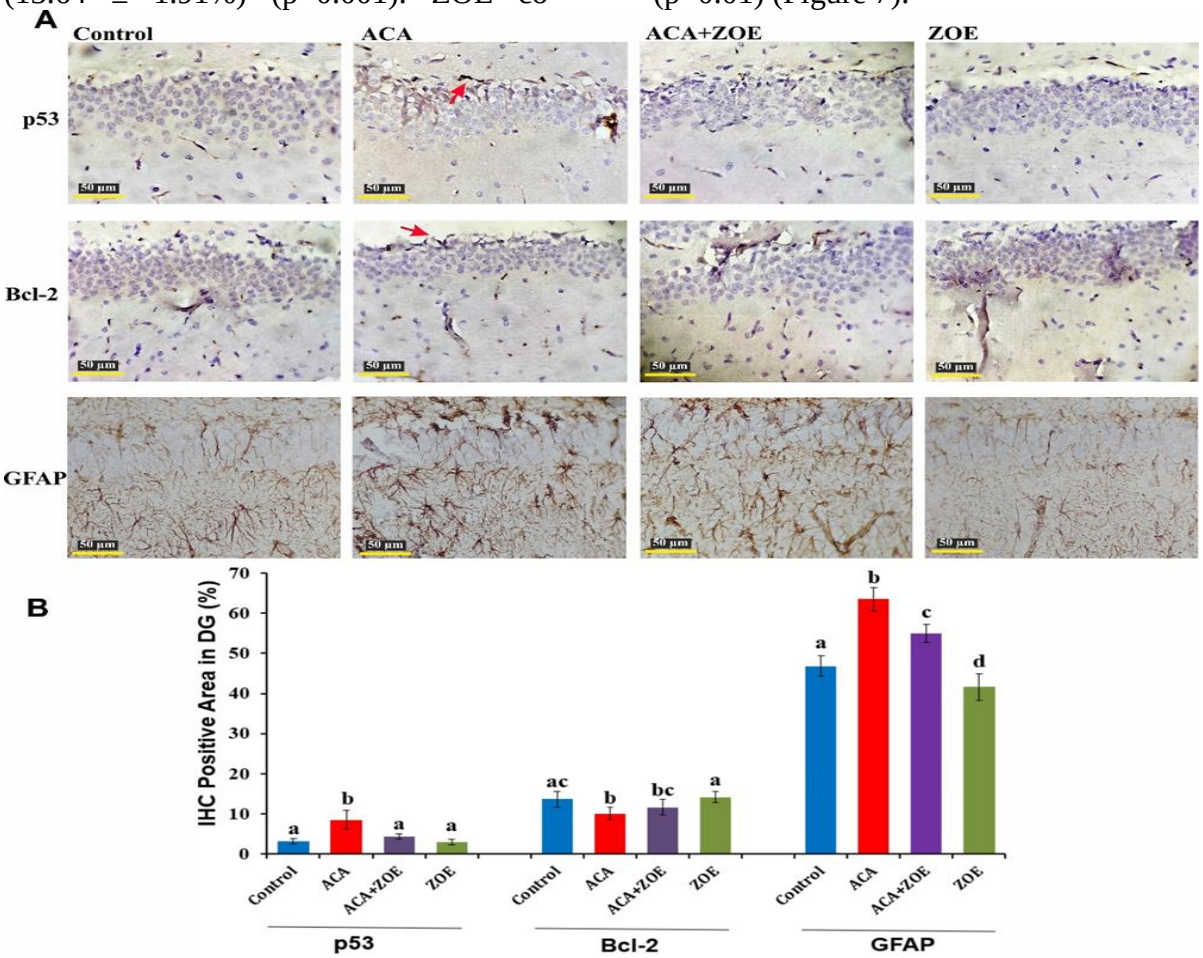

Figure 7. Immunohistochemical (IHC) analysis of p53, Bcl-2, and GFAP expression in the dentate gyrus (DG) region following chronic acrylamide (ACA) exposure and/or *Zingiber officinale* extract (ZOE) administration. (A) Representative photomicrographs showing p53, Bcl-2, and GFAP immunoreactivity in the DG across the experimental groups: Control, ACA, ACA+ZOE, and ZOE. ACA-treated rats showed marked increases in p53 and GFAP immunopositivity compared to controls, whereas Bcl-2 expression was reduced. Co-treatment with ZOE attenuated ACA-induced p53 and GFAP overexpression and partially restored the Bcl-2 levels. ZOE alone did not markedly alter the expression profile compared to that of the control. Red arrows indicate shrunken neurons with necrosis and pyknotic nuclei (magnification ×400; scale bar = 50 µm). (B) Quantification of the IHC-positive area (%) for each marker in the dentate gyrus (DG). Data are presented as the mean ± standard deviation. Different lowercase letters (a, b, and c) indicate statistically significant differences among groups (one-way ANOVA followed by Tukey's post-hoc test, $p<0.05$).

Effect of ZOE on p53, Bcl-2, and GFAP expression after ACA-induced PC neurotoxicity

In the parietal cortex (PC), ACA exposure significantly increased p53 positivity (10.05 ± 1.66%) compared to that in the control group (2.23 ± 0.76%) ($p<0.001$). ZOE co-administration reduced this to 2.51 ± 0.54%, comparable to the control values ($p > 0.001$), and the ZOE-only group exhibited the lowest expression (1.70 ± 0.27%). In the parietal cortex, ACA induced a pronounced decrease in Bcl-2 expression (5.54 ± 1.52%) compared to that in the control group (14.26 ± 1.69%) ($p<0.001$). ZOE co-administration increased Bcl-2 levels to 9.95 ± 1.76% ($p < 0.001$ vs. ACA), although the levels remained lower than those in the control group ($p < 0.001$). The ZOE-only group exhibited the highest Bcl-2 expression (15.80 ± 1.43%). In the parietal cortex, GFAP expression was significantly higher in the ACA group (57.31 ± 3.21%) than in the control group (43.29 ± 2.69%) ($p < 0.001$). Although ZOE co-treatment slightly lowered GFAP levels (54.14 ± 3.24%), this reduction was not statistically significant ($p>0.05$). The ZOE-only group showed lower GFAP expression than the control group (39.13 ± 1.87%) ($p<0.05$) (Figure 8).

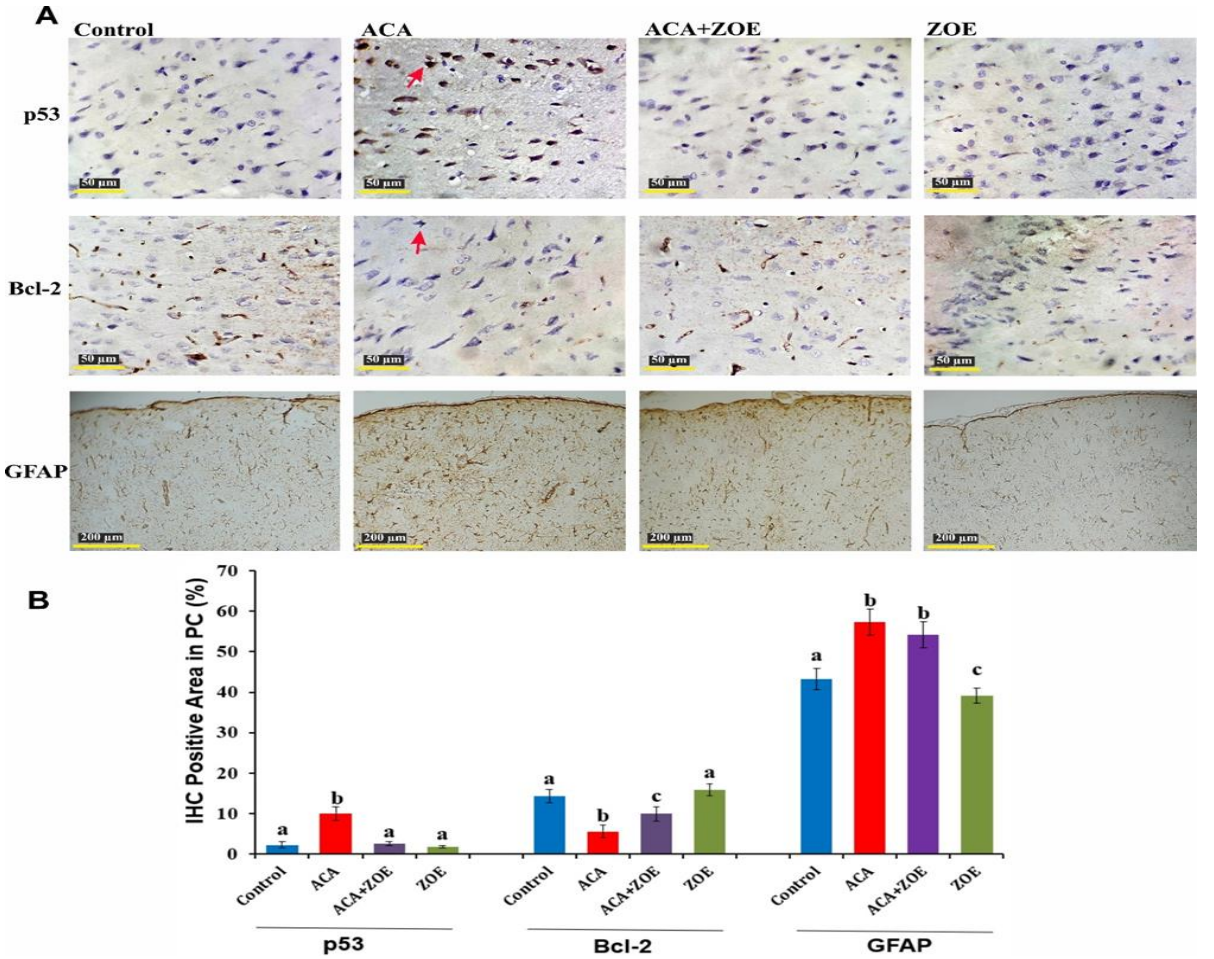

Figure 8. Immunohistochemical (IHC) analysis of p53, Bcl-2, and GFAP expression in the parietal cortex (PC) following chronic acrylamide (ACA) exposure and/or *Zingiber officinale* extract (ZOE) administration. (A) Representative photomicrographs of p53, Bcl-2, and GFAP in the cortex of the control, ACA, ACA+ZOE, and ZOE groups. ACA increased p53 and GFAP levels and decreased Bcl-2 levels compared to the control. ZOE co-treatment reduced p53 and GFAP overexpression and partially restored the Bcl-2 levels. Red arrows indicate shrunken neurons with necrosis and pyknotic nuclei (magnification ×400 and ×100; scale bar = 50 µm and 100 µm). (B) Quantification of the IHC-positive area (%) for each marker in the parietal cortex (PC). Data are presented as the mean ± standard deviation. Different lowercase letters (a, b, and c) indicate statistically significant differences among groups (one-way ANOVA followed by Tukey's post-hoc test, $p<0.05$).

Discussion

The present study provides comprehensive behavioral, biochemical, histomorphometric, and immunohistochemical evidence that chronic exposure to ACA induces significant spatial memory acquisition impairment, oxidative stress, neuronal loss, and alterations in apoptosis- and gliosis-related markers in the hippocampus and parietal cortex of rats. More importantly, co-administration of ZOE partially or completely attenuated these deleterious changes, underscoring its potential as a neuroprotective agent against environment-induced neurotoxicity.

In our study, ACA exposure led to significant impairments in spatial learning and memory, as evidenced by the increased escape latency and reduced probe performance. These findings align with previous *in vivo* reports that ACA disrupts hippocampal synaptic plasticity and long-term potentiation (Izumi et al. 2022). The marked behavioral recovery observed in the ACA+ZOE group represents a novel demonstration of the ability of *Z. officinale* to mitigate ACA-induced cognitive deficits. Although previous studies have described the antioxidant and anti-apoptotic potential of ginger, our integrated behavioral, histological, and molecular data provide direct *in vivo* evidence of its neuroprotective efficacy against chronic ACA exposure. Additionally, mechanistic reviews of ACA neurotoxicity underscore its ability to provoke oxidative stress, apoptosis, and neuroinflammation, pathways strongly implicated in spatial memory decline across experimental models (Ghasemzadeh Rahbardar et al. 2021; Zhao et al. 2022). The hippocampus, particularly the CA1, CA3, and dentate gyrus (DG) subregions, is notably vulnerable to oxidative insults, impairing synaptic plasticity and structural integrity essential for learning and memory (Salim 2017). This heightened susceptibility may underlie the behavioral deficits observed in ACA-treated rats. Interestingly, co-administration of ZOE markedly reduced escape latency and enhanced memory retention, with performance nearly equivalent to that of the control group at the end of the acquisition phase. These improvements are likely attributable to the neuroprotective properties of ginger's principal phytochemicals—6-gingerol and 6-shogaol—which have been reported to enhance neurotrophic factor expression, promote synaptic plasticity, and stimulate neurogenesis, all of which are critical processes for learning and memory Moreover, the well-documented antioxidant, anti-inflammatory, and anti-apoptotic activities of ginger extract, particularly through the modulation of oxidative stress pathways and preservation of neuronal structural integrity, further support its potential to enhance spatial memory (Mohd Sahardi and Makpol 2019). The absence of spatial memory impairment in animals treated with ZOE alone underscores the safety and therapeutic promise of this botanical intervention. A limitation of the present behavioral analysis is that distance traveled and path efficiency were not quantified, despite being available in the tracking software. These measures could have provided additional confirmation of navigation strategies. Nonetheless, the absence of significant differences in swim velocity during the acquisition and probe phases strongly suggests that the impaired performance of ACA-treated animals was attributable to spatial memory deficits rather than locomotor dysfunction. Although ACA is a well-established peripheral nervous system toxicant associated with hindlimb weakness and gait abnormalities in chronic exposure models (Bai et al. 2021), in the present study, only a slight reduction in swimming speed was observed in ACA-treated rats during the early testing phase, indicating minor motor involvement. However, stable swimming velocities in later sessions and pronounced deficits in escape latency and probe performance strongly indicate that the predominant neurotoxic effects under

the current dosing regimen were central, specifically affecting spatial learning and memory. These results align with studies reporting that acrylamide-induced neurotoxicity can differentially affect central nervous system (CNS) and peripheral nervous system (PNS) domains depending on dose, duration, and route of exposure.

Biochemical assays revealed that ACA exposure significantly decreased TAC and increased TOS and OSI, indicating a shift toward a pro-oxidative state. This redox imbalance is consistent with ACA known ability of ACA to generate ROS and deplete endogenous antioxidants, such as glutathione (GSH) and superoxide dismutase (SOD) (Zhao et al. 2022; Moradi et al. 2025b). Oxidative stress not only damages cellular macromolecules but also initiates mitochondrial-mediated apoptotic cascades, contributing to neurodegeneration (Dash et al. 2025). ZOE co-treatment restored TAC levels, reduced TOS, and normalized OSI, suggesting potent antioxidant effects. The polyphenolic constituents of ginger may not only directly scavenge ROS and chelate metal ions, but also enhance endogenous antioxidant defenses, possibly via Nrf2-mediated pathways, as suggested by previous studies (Ayustaningwarno et al. 2024). This dual mode of action, direct radical neutralization and activation of cellular antioxidant pathways, likely accounts for the observed biochemical recovery.

ACA treatment induced marked reductions in pyramidal cell layer thickness in the CA1 and CA3 regions and in the granular and molecular layers of the DG. Neuronal density was also significantly decreased across all hippocampal subregions, in agreement with earlier histopathological studies documenting ACA-induced hippocampal atrophy and neuronal loss (Lee et al. 2018). Such structural deterioration directly correlates with deficits in learning and memory, as hippocampal integrity is essential for encoding and retrieving spatial information. Co-administration of ZOE significantly preserved layer thickness and neuronal density, and in some cases, restored these values to control levels. Furthermore, the observed neuroprotection may involve the modulation of pro-survival signaling cascades, such as PI3K/Akt and ERK1/2. However, these mechanisms were not directly assessed in the present study and warrant further investigation (Angelopoulou et al. 2022; Razak et al. 2023). In other chemically induced neurotoxicity paradigms, ginger and its bioactive constituents attenuated reactive oxygen species generation, preserved neuronal architecture, and improved spatial memory (Marefati et al. 2021; Zahedi et al. 2025). The present study extends these observations by concurrently demonstrating behavioral, histological, biochemical, and molecular protection in a chronic ACA exposure model, thereby providing broader mechanistic evidence for the neurotherapeutic potential of *Z. officinale*.

ACA exposure led to a marked upregulation of p53, a pivotal pro-apoptotic transcription factor, and a concomitant downregulation of Bcl-2, a key anti-apoptotic protein, within the CA1, CA3, and DG subregions of the hippocampus, as well as the parietal cortex. These alterations are characteristic of the intrinsic (mitochondrial) apoptotic pathway, wherein p53 activation facilitates the translocation of pro-apoptotic Bcl-2 family proteins, such as Bax, to the mitochondrial outer membrane, triggering mitochondrial outer membrane permeabilization (MOMP), the subsequent release of cytochrome c into the cytosol, apoptosome assembly, and activation of downstream caspases, ultimately culminating in programmed cell death. Both *in vitro* and *in vivo* studies have corroborated the association between ACA exposure and increased p53 expression, demonstrating that p53 upregulation coincides with oxidative DNA damage, mitochondrial

dysfunction, and neuronal apoptosis in experimental models of ACA neurotoxicity (Luo et al. 2022; Wang et al. 2025).

Concomitantly, ACA exposure markedly increased the expression of GFAP, a canonical marker of reactive astrogliosis. While transient astrocyte activation can provide neuroprotection through metabolic support, antioxidant defense, and glutamate clearance, sustained or excessive astrogliosis promotes a maladaptive phenotype characterized by pro-inflammatory cytokine release, disruption of synaptic homeostasis, and amplification of neurodegenerative processes (Li et al., 2019; Qian et al. 2023). ZOE co-treatment markedly attenuated ACA-induced upregulation of p53 and GFAP, while partially restoring Bcl-2 expression. These findings indicate that ZOE mitigates ACA-induced apoptosis and astrocytic activation rather than fully normalizing them. As described in previous studies, the bioactive constituents of ginger have been shown to regulate apoptotic protein expression by inhibiting the NF-κB and p38 MAPK pathways, thereby preventing mitochondrial dysfunction and caspase activation. Furthermore, these phytochemicals can reduce astrocytic activation by limiting the release of pro-inflammatory cytokines such as tumor necrosis factor-alpha (TNF-α), interleukin-1 beta (IL-1β), and IL-6, ultimately mitigating neuroinflammatory cascades (Tondro et al. 2022; Priyadarshini et al. 2025). The neuroprotective effects of ZOE observed in this study likely resulted from partial modulation of oxidative stress, apoptotic signaling, and astrocytic activation. Such attenuation, rather than full normalization, may provide substantial functional recovery in chronic neurotoxicity. These include direct antioxidant activity for ROS scavenging and prevention of oxidative damage, activation of Nrf2/ARE signaling to boost endogenous antioxidant enzymes, anti-apoptotic modulation by restoring the Bcl-2/p53 balance, preventing Bax translocation, and inhibiting cytochrome c release, and anti-inflammatory action through suppression of GFAP-linked astrocyte reactivity and pro-inflammatory cytokines. Additionally, ZOE may enhance synaptic plasticity and neuronal survival by modulating neurotransmitter systems and upregulating neurotrophic factors, such as brain-derived neurotrophic factor (BDNF), collectively preserving spatial memory under ACA-induced neurotoxic stress. These mechanisms likely act in concert, rather than in isolation, to maintain neuronal integrity and sustain spatial memory performance in the face of ACA-induced neurotoxicity.

Although our results strongly support the neuroprotective potential of ZOE, several limitations should be acknowledged. This study was conducted exclusively in male rats; therefore, potential sex-related differences in ACA neurotoxicity or ZOE responsiveness remain unexplored. Only single doses of ACA and ZOE were tested, and dose–response relationships were not evaluated, limiting the extrapolation of the findings. Specific neurotrophic factors (e.g. BDNF), synaptic proteins (e.g. synaptophysin), and inflammatory cytokines have not been assessed, and the pharmacokinetics and brain bioavailability of ginger constituents remain unclear. Future studies should address these points and evaluate the long-term outcomes to better elucidate the translational relevance of the neuroprotective effects of ZOE.

This study demonstrates that ZOE effectively mitigates ACA-induced spatial memory acquisition deficits, oxidative stress, neuronal loss, and dysregulation of apoptosis- and gliosis-related markers in the hippocampus and parietal cortex of rats. These findings highlight ZOE as a promising candidate for the prevention or treatment of environmental chemical–induced neurotoxicity, warranting further investigation in translational and clinical research.

Acknowledgment

We sincerely thank the Department of Pharmacology, School of Veterinary Medicine, Shiraz University, for their valuable assistance in the preparation of the *Zingiber officinale* extract used in this study.

Conflicts of interest

The authors have declared that there is no conflict of interest.

Funding

The authors are deeply grateful to the Research Council of Shiraz University for their generous financial support (Grant No. 2PRB1M376959).

Ethical Considerations

This study adhered to the ARRIVE guidelines and received ethical approval from the Ethical Committee of Shiraz University (Shiraz, Iran).

Code of Ethics

The ethical code for this study is ID IR.USREC.1403.015.

Authors' Contributions

H. R. M. Conceptualization; Methodology; Investigation; Formal analysis; Data curation; Visualization; Writing – original draft; Writing – review and editing; Project administration; Funding acquisition. Z. Kh. Project administration; Investigation; Writing – review and editing. F. A. Methodology; Investigation; Formal analysis; Data curation. S. F. Methodology; Investigation; Data curation. M. T. Investigation; Data curation; Writing – review and editing. M. R. Methodology; Investigation; Data curation. M. Kh. Investigation; Data curation.

Abbreviations

ACA: Acrylamide. ZOE: Zingiber officinale extract. ROS: Reactive oxygen species. LH: Luteinizing Hormone. BCL2: B-cell lymphoma-2. TAC: Total antioxidant capacity. TOS: Total oxidant status. OSI: Oxidative stress index. DG: Dentate gyrus. MWM: Morris water maze. H_2O_2: Hydrogen peroxide. $FeCl_3$: Ferric chloride. HCl: Hydrochloric acid. FRAP: Ferric reducing antioxidant power. IHC: Immunohistochemical. GFAP: Glial fibrillary acidic protein. SD: Standard deviation. SPSS: Statistical package for social sciences. H&E: Hematoxylin and Eosin. PC: Parietal cortex. GSH: Glutathione. SOD: Superoxide dismutase. MOMP: Mitochondrial outer membrane permeabilization. DAB: 3,3′-diaminobenzidine. PMSF: phenylmethylsulfonyl fluoride RIPA: Radioimmunoprecipitation assay. SDS: Sodium dodecyl sulfate. CNS: Central nervous system. PNS: Peripheral nervous system. TNF-α: Tumor necrosis factor-alpha. IL: Interleukin. BDNF: Brain-derived neurotrophic factor.

References

Abd Al Haleem EN, Hasan WYS, Arafa HMM (2022) Therapeutic effects of thymoquinone or capsaicin on acrylamide-induced reproductive toxicity in rats mediated by their effect on oxidative stress, inflammation, and tight junction integrity. Drug Chem Toxicol 45(5):2328-2340.

Ahmadi M, Taherianfard M, Shomali T (2019) Zataria multiflora could improve hippocampal tau protein and TNF(α) levels and cognitive behavior defects in a rat model of Alzheimer's disease. Avicenna J Phytomed 9(5):465-473.

Alshaer Sh, Mohammad AA, Feras DE, Reem AT (2025) Investigating the potential effects of olive leaves and ginger rhizome extracts on kidney and liver functions in alloxan-induced diabetic rats. Avicenna J Phytomed 15: 1124.

Angelopoulou E, Paudel YN, Papageorgiou SG, Piperi C (2022) Elucidating the beneficial effects of ginger (Zingiber officinale Roscoe) in Parkinson's disease. ACS Pharmacol Transl Sci 5(10):838-848.

Arcusa R, Villaño D, Marhuenda J, Cano M, Cerdà B, Zafrilla P (2022) Potential Role of Ginger (Zingiber officinale Roscoe) in the

Prevention of Neurodegenerative Diseases. Front Nutr 9:809621.

Ayustaningwarno F, Anjani G, Ayu AM, Fogliano V (2024) A critical review of Ginger's (Zingiber officinale) antioxidant, anti-inflammatory, and immunomodulatory activities. Front Nutr 11:1364836.

Bai Y, Gu Z, Zhang T, et al. (2021) Toxic effects of subacute exposure to acrylamide on motor endplates of the gastrocnemius in rats. Toxicol 462:152934.

Bostanifard M, Moradi HR, Khaksar Z, Abbasi S, Hadavand BS, Faraji M (2026) Transplacental and lactational transfer of polystyrene nanoplastics leads to long-term ovarian impairment in rat offspring. J Hazard Mater Adv 2026:101007.

Bradford MM (1976) A rapid and sensitive method for the quantitation of microgram quantities of protein utilizing the principle of protein-dye binding. Anal Biochem 72:248-54.

Dash UC, Bhol NK, Swain SK, et al. (2025) Oxidative stress and inflammation in the pathogenesis of neurological disorders: Mechanisms and implications. Acta Pharm Sin B 15(1):15-34.

Ghasemzadeh Rahbardar M, Cheraghi Farmad H, Hosseinzadeh H, Mehri S (2021) Protective effects of selenium on acrylamide-induced neurotoxicity and hepatotoxicity in rats. Iran J Basic Med Sci 24(8):1041-1049.

Gholampour F, Fatemeh BGH, Seyed MO, Jaafar V (2017) The protective effect of hydroalcoholic extract of Ginger (Zingiber officinale Rosc.) against iron-induced functional and histological damages in rat liver and kidney. Avicenna J Phytomed 7: 542.

Gomez-Pinilla F, Hillman C (2013) The influence of exercise on cognitive abilities. Compr Physiol 3(1):403-28.

Haidari F, Majid M, Behnaz A, Mehdi Z, Mojdeh F (2020) Cinnamon extract supplementation improves inflammation and oxidative stress induced by acrylamide: An experimental animal study. Avicenna J Phytomed 10: 243.

Hosseinkhani F, Hosseinifar S, Tabandeh MR (2024) Dimethyl itaconate mitigates histological distortions, inflammation, and oxidative stress in the rat model of polycystic ovary syndrome. J Steroid Biochem Mol Biol 243:106546.

Huchthausen J, Escher BI, Grasse N, König M, Beil S, Henneberger L (2023) Reactivity of Acrylamides causes cytotoxicity and activates oxidative stress response. Chem Res Toxicol 36(8):1374-1385.

Izumi Y, Fujii C, O'Dell KA, Zorumski CF (2022) Acrylamide inhibits long-term potentiation and learning involving microglia and pro-inflammatory signaling. Sci Rep 12(1):12429.

Lee S, Park HR, Lee JY, et al. (2018) Learning, memory deficits, and impaired neuronal maturation attributed to acrylamide. J Toxicol Env Heal A 81(9):254-265.

Li K, Li J, Zheng J, Qin S (2019) Reactive astrocytes in neurodegenerative diseases. Aging Dis 10(3):664-675.

Luo Q, Sun W, Wang YF, Li J, Li DW (2022) Association of p53 with Neurodegeneration in Parkinson's Disease. J Parkinsons Dis 2022(1):6600944.

Marefati N, Abdi T, Beheshti F, Vafaee F, Mahmoudabady M, Hosseini M (2021) Zingiber officinale (Ginger) hydroalcoholic extract improved avoidance memory in rat model of streptozotocin-induced diabetes by regulating brain oxidative stress. Horm Mol Biol Clin Investig 43(1):15-26.

Mohd Sahardi NFN, Makpol S (2019) Ginger (Zingiber officinale Roscoe) in the prevention of ageing and degenerative diseases: Review of current evidence. Evid Based Complement Alternat Med 2019(1):5054395.

Moradi HR, Kazemipour N, Nazifi S, Khodayari M, Samadi L, Yousefi A (2025a) Protective effects of wheat sprout extract on acrylamide-induced toxicity in testis, prostate gland and sperm parameters of rats. J Mol Histol 56(3):137.

Moradi HR, Vafaeyan A, Khaksar Z, Alipour F (2026) Protective effects of wheat sprouts extract against acrylamide-induced skin toxicity: Modulation of oxidative stress, apoptosis, and histomorphometric alterations in rats. ESPR 2026:1-13.

Moradi HR, Khaksar Z, Alipour F, Fathollahi S, Divar M-R, Rashidi M (2025b) Protective role of Zingiber officinale extract on acrylamide-induced toxicity in rat testes: Immunohistochemical, histomorphological, biochemical, and sperm analysis. Andrologia

2025(1):9324806.
Mortazavi Z, Mahboobeh GR, Soghra M, Hossein H (2025) Protective role of zeaxanthin on acrylamide-induced neurotoxicity in Wistar rats. Avicenna J Phytomed 15: 1016.
Negah SS, Moradi HR, Forouzanfar F, Sahraian MA, Faraji M (2025) The role of small extracellular vesicles derived from glial cells in the central nervous system under both normal and pathological conditions. Neurochem Res 50(2):89.
Ojo AO, Omowumi HE, Oluwabukunmi MO, Olatunbosun OO, Lawrence DA, Olufemi IO, Emmanuel OT, Abiodun A (2021) The effect of ginger (Zingiber officinale) feed on cardiac biomarker in medium-dose isoproterenol-induced myocardial toxicity. Avicenna J Phytomed 11:1.
Priyadarshini S, Goyal K, R R, et al. (2025) Polypharmacology and neuroprotective effects of gingerol in Alzheimer's disease. Mol Neurobiol 62(7):8166-8186.
Qian K, Jiang X, Liu Z-Q, et al. (2023) Revisiting the critical roles of reactive astrocytes in neurodegeneration. Mol Psychiatry 28(7):2697-2706.
Razak AM, Tan JK, Mohd Said M, Makpol S (2023) Modulating Effects of Zingiberaceae Phenolic Compounds on Neurotrophic Factors and Their Potential as Neuroprotectants in Brain Disorders and Age-Associated Neurodegenerative Disorders: A Review. Nutrients 15(11):2564.
Salim S (2017) Oxidative Stress and the Central Nervous System. J Pharmacol Exp Ther 360(1):201-205.
Save E, Paz-Villagran V, Alexinsky T, Poucet B (2005) Functional interaction between the associative parietal cortex and hippocampal place cell firing in the rat. Eur J Neurosci 21(2):522-30.
Shalaby MA, Hamowieh AR (2010) Safety and efficacy of Zingiber officinale roots on fertility of male diabetic rats. Food Chem Toxicol 48(10):2920-4.
Shoaib S, Ansari MA, Fatease AA, et al. (2023) Plant-derived bioactive compounds in the management of neurodegenerative disorders: Challenges, future directions and molecular mechanisms involved in neuroprotection. Pharmaceutics 15(3).
Tandisehpanah Z, Amir F, Ali A, Mahboobeh GR, Bibi MR, Hossein H (2022) Protective effect of aqueous and ethanolic extracts of Lippia citriodora Kunth. on acrylamide-induced neurotoxicity. Avicenna J Phytomed 12:281.
Tondro G, Rajabzade G, Mohammadi A, Moradi H, Sahab Negah S (2022) Anti-inflammatory effects of nano-curcumin on a glioblastoma cell line. Shefaye Khatam 10(3):48-56.
Wang Y, Liu Y, Zhang X, et al. (2025) Acrylamide induces antiapoptotic autophagy and apoptosis by activating PERK pathway in SH-SY5Y cells. Toxics 13(1).
Zahedi E, Naseri FM, Zamani E, et al. (2025) Ginger Extract improves cognitive dysfunction via modulation of gut microbiota-derived short-chain fatty acids in D-galactose/ovariectomy-induced Alzheimer-like disease. Mol Neurobiol 62(4):5095-5108.
Zhang X, Jonas P (2020) Integration of spatial and non-spatial information by heterogeneous dentate gyrus granule cells. J Life Sci (Westlake Village) 2(4):19-24.
Zhao M, Zhang B, Deng L (2022) The Mechanism of Acrylamide-Induced Neurotoxicity: Current Status and Future Perspectives. Front Nutr 9:859189.
Zhao X, van Praag H (2020) Steps towards standardized quantification of adult neurogenesis. Nat Commun 11(1):4275.